Research Article

Yongbo Wang, Peng Gao*, Huaizhi Su, Yuanyu Qin, Yimeng Wang, and Gang Xue

Failure criteria and microstructure evolution mechanism of the alkali–silica reaction of concrete

https://doi.org/10.1515/rams-2023-0102
received January 19, 2023; accepted July 14, 2023

Abstract: In this study, the influence of two distinct reactive aggregate dosages on the alkali–silica reaction (ASR) of concrete was investigated. The expansion ratio, axial compressive strength, splitting tensile strength, and relative dynamic elastic modulus (RDEM) of concrete were considered as the main parameters to study the failure criteria of concrete induced by ASR at 40°C. Microscopic experiments, such as scanning electron microscopy and X-ray computed microtomography, were applied to analyze the damage induced by ASR on the concrete prisms and the propagation of internal cracks of the reactive aggregates in nanospace. The results showed that the two ranges can be used as the failure criteria produced by the ASR of concrete containing 3 and 6% dosages of reactive aggregates at 40°C, respectively, when the RDEM of concrete was reduced to 70–75% and 85–90%. Additionally, the results of CT indicated that microcracks tended to extend from the initial defects of aggregate to the cement slurry. Meanwhile, ASR gel packed with the pores, which reduced the porosity. It was noteworthy that the adhesive force between the ASR gel and the cement matrix after filling pores could not make up for the loss of the mechanical properties of concrete.

Keywords: alkali–silica reaction, mechanical properties, failure criteria, deterioration mechanism, X-ray computed microtomography, microstructure

1 Introduction

Alkali–aggregate reaction (AAR) is a common factor affecting the durability of concrete structures [1]. According to the types of alkali-active aggregates, the AAR can be divided into two types, including alkali–silica reaction (ASR) and alkali–carbonate rock reaction [2,3]. ASR is recognized as one of the most deleterious phenomena in concrete, which will lead to serviceability problems, cracks, and other deterioration mechanisms [4]. Since it was discovered in the 1940s, the damage of ASR has been highly valued by countries all over the world because of its long reaction period and strong destructiveness [5].

ASR is a deleterious reaction that takes place between alkali and silica contained in reactive aggregate and produces hydrophilic gel [6]. In a high relative humidity environment, the gel can absorb water and produce expansion pressure inside the material. The determinants (yield stress and viscosity) are the important rheological properties of ASR gels [7]. The gel with high yield stress and viscosity will produce expansion pressure on pores and tensile stress in concrete. When the expansion pressure is higher than the tensile stress, microcracks will be generated in the aggregate particles [7,8]. As the ASR progresses, the gel penetrates into the cracks and spreads into the cement paste [9,10], which eventually leads to an increase in expansion pressure,

* **Corresponding author: Peng Gao,** School of Civil Engineering, Inner Mongolia University of Science and Technology, Baotou, Inner Mongolia, 014010, China; Intelligent Construction and Operation Engineering Research Center at Universities of Inner Mongolia Autonomous Region, Inner Mongolia University of Science and Technology, Baotou, Inner Mongolia, 014010, China; Construction Structure Disaster Prevention and Mitigation Engineering Technology, Research Center of Inner Mongolia Autonomous Region, Inner Mongolia University of Science and Technology, Baotou, Inner Mongolia, 014010, China,
e-mail: gaop182@163.com
Yongbo Wang, Yuanyu Qin, Yimeng Wang: School of Civil Engineering, Inner Mongolia University of Science and Technology, Baotou, Inner Mongolia, 014010, China
Huaizhi Su: The National Key Laboratory of Water Disaster Prevention, Hohai University, Nanjing 210098, China; College of Water Conservancy and Hydropower Engineering, Hohai University, Nanjing 210098, China
Gang Xue: School of Civil Engineering, Inner Mongolia University of Science and Technology, Baotou, Inner Mongolia, 014010, China; Intelligent Construction and Operation Engineering Research Center at Universities of Inner Mongolia Autonomous Region, Inner Mongolia University of Science and Technology, Baotou, Inner Mongolia, 014010, China; Construction Structure Disaster Prevention and Mitigation Engineering Technology Research Center of Inner Mongolia Autonomous Region, Inner Mongolia University of Science and Technology, Baotou, Inner Mongolia, 014010, China

Open Access. © 2023 the author(s), published by De Gruyter. This work is licensed under the Creative Commons Attribution 4.0 International License.

resulting in large-area cracking of the concrete and a subsequent decrease in the strength and stiffness of concrete structure [11,12]. The ASR progress can be better represented by Figure 1.

The damage caused by ASR to concrete is mainly reflected in the decline of the bearing capacity of concrete structures [13–15]. Several attempts have been made on this by scholars to evaluate the influence of ASR development on concrete materials and mechanical properties all over the world [1–3,5,16–18]. Pan *et al.* [13] established the mesoscopic particle model of ASR in concrete and conducted uniaxial compression tests to evaluate the damage of ASR in concrete. They reported that the tensile stress was produced in cement paste with the continuous progress of ASR, which eventually finally reached the meso-strength of material after continuous accumulation. The cement paste cracked as a result of accumulating tensile stresses that were greater than the components could withstand, which caused the concrete to deteriorate even further. As the curing age increased, several researchers found that ASR caused a reduction in the compressive and tensile strength of concrete [2,3,15]. The tensile strength of concrete is very low, making it liable to collapse, particularly in the ASR phenomenon where the tensile strength of the concrete is easily affected [5]. In addition, it was found that the gain in concrete strength with time must be considered when evaluating the effect of ASR on the strength of concrete [16].

Some researchers [17] found that the expansion related to ASR exhibited no significant impact on the reduction of the uniaxial compressive strength of concrete. However, when the concrete contains a certain amount of high reactive aggregates, the uniaxial compressive strength of concrete declines significantly [3,5,15,18]. Ahmed *et al.* [15] studied the effect of ASR on the degradation trend of mechanical properties of concrete, and the compressive strength, direct tensile strength, splitting tensile strength (STS), and static elastic modulus of concrete were regarded as mechanical indexes. The results showed that ASR showed a negative effect on the mechanical properties of concrete, and the expansion caused by ASR had less influence on the direct tensile strength of concrete in the early stage than the STS and flexural strength of concrete. Compared with the compressive strength, the static elastic modulus was a sensitive and reliable indicator to reflect the deterioration degree of concrete due to ASR.

These studies showed that due to the different test methods of the reactivity of aggregate and the mechanical properties of concrete, this reduction induced by ASR in different types of aggregates and different mechanical properties was different [5,14]. While the elastic modulus of concrete is a good indicator for evaluating internal damage caused by ASR because of its high sensitivity to microcracks [5,12,14], Abd-Elssamd *et al.* [16] found a logarithmic correlation with the correlation coefficient (R^2 = 0.9) between the modulus of elasticity and volume expansion at high expansion ratio (ER). As the decrease of the ER of ASR (the high ER was 0.62, and the slow ER was 0.6), the R^2 value also decreased to 30% because of the hydration of cement and the creep of cement paste. When the ER value of concrete only reached 0.6%, the elastic modulus of concrete might also drop sharply to around 30% of the initial value [14]. It is worth noting that the mechanical properties of concrete affected by ASR exhibited a direction dependence with the anisotropic degradation of concrete mechanical properties. A multi-axis compression test conducted by Comi confirmed the characteristics of reduced expansion in the direction of the major stress of compression, and the elastic modulus measured along the direction of constraint was significantly more affected by ASR than compressive strength [19]. The elastic modulus' susceptibility to anisotropy has also been documented. When compared to concrete's compressive strength, Anca discovered that the anisotropy of the elastic modulus appeared to be more noticeable [20]. In addition, to investigate the best indicators to characterize the degree of ASR injury, Liu *et al.* [21] conducted tests on the dynamic elastic modulus, the compressive strength, the STS, and the flexural strength of specimens in different periods. Experiment results indicated that the influence of ASR on the compressive strength of concrete was less than that on the STS and flexural strength of

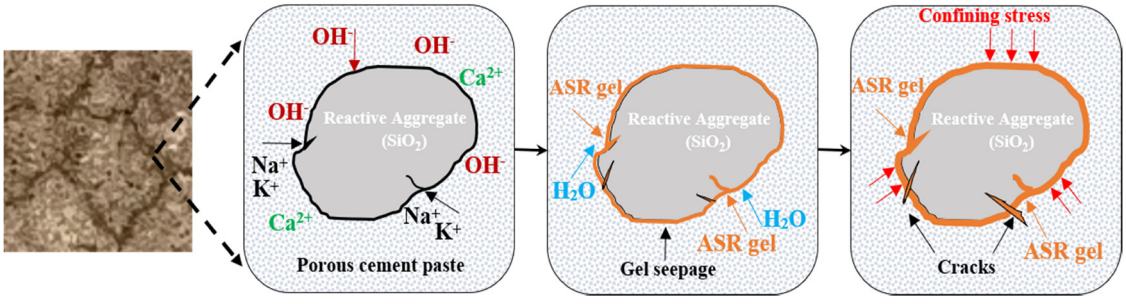

Figure 1: Schematic demonstration of the ASR progress.

concrete and found that the dynamic elastic modulus of concrete had a linear relationship with its ER. Additionally, Swamy [22] used the dynamic elastic modulus and ultrasonic pulse velocity to detect the ASR damage inside the concrete as he looked into the finest indications to describe the severity of the injury. The results [22] had clearly shown that the dynamic elastic modulus was more appropriate to the ASR damage in concrete (shown in Figure 2).

In addition, the deterioration degree induced by ASR is not only related to the types of reactive aggregate [18,23], and its chemical and physical characteristics [10,11,15,23] but also related to the amount of reactive aggregate [24]. Also, a small amount of reactive aggregate could produce ASR-related damages in concrete [22]. Therefore, many scholars investigated the influence of reactive aggregate and other factors on the mechanical properties of concrete and also adopted various measures to alleviate the expansion induced by ASR [2,3,5]. The most common method to inhibit ASR is the application of supplementary cementitious materials (SCMs), mainly using fly ash, metakaolin, silica fume, *etc.* [1,3,5,25]. Due to the existence of the volcanic ash effect, SCMs effectively consume CH, which helps to form additional calcium silicate hydrate (C-S-H) and combines more alkali ions, thus helping to lower the alkali content of concrete. In addition to reactive silica, the alkali is also an indispensable reactant in ASR, so incorporating SCMs into concrete can be considered a practical approach to inhibiting ASR in concrete.

The purpose of this study aimed to explore the ASR failure criteria of concrete with two various dosages of reactive aggregates. At present, there are many measures to inhibit the ASR in concrete. However, only a few studies have investigated the evolution of mechanical properties of concrete and its failure criteria caused by ASR with different dosages of reactive aggregates. In this article, the axial compressive strength (ACS), STS, and RDEM tests were carried out on concrete with different contents of reactive aggregates. Simultaneously, the relationship between the RDEM, other indicators, and the ER of concrete prisms at different ages was analyzed, and the failure criteria of concrete affected by ASR were established based on the RDEM loss of concrete. Besides, in order to better understand the development process of ASR and analyze the relationship between the degradation of mechanical properties and crack development, scanning electron microscopy (SEM) combined with energy-dispersive X-ray spectral (EDS) was applied to analyze the changes in product morphology and element composition at the interface between cement paste and aggregate at different ages. The phases of the hydration products were also evaluated by X-ray diffractometer (XRD), and X-ray computed microtomography (X-ray CT) was carried out to explore porosity and the crack evolution inside the concrete. Therefore, these results will be highly significant in determining the damage degree of ASR to concrete in the future, which will provide theoretical guidance and a technical basis for studying the degree of damage to concrete caused by ASR.

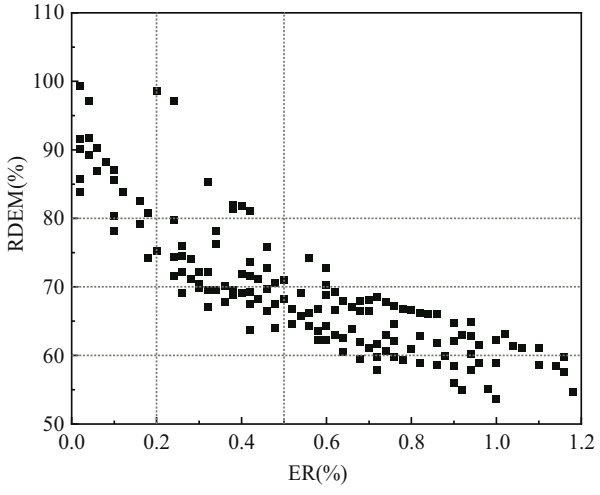

Figure 2: Relationship between the ER of ASR and relative dynamic elastic modulus (RDEM) of concrete [22].

2 Experimental

2.1 Raw materials

The physical properties and chemical composition of ordinary Portland cement are listed in Tables 1 and 2. And the qualified stability indicates that the expansion degree of cement measured by Lei's method met the requirements of GB/T 1346-2011 [26].

The non-reactive fine aggregates intended for use in concrete were natural mid-sand, and the quartz glass aggregates with 99.91% SiO_2 were considered reactive aggregates. The chemical compositions of quartz glass aggregate are shown in Table 3, and the gradation of mid-sand and coarse aggregates met the requirements in the SL352-2020 standard [27] and GB/T 14685-2011 [28], respectively. And piped water was used to mix the specimens.

2.2 Mixture proportions

The prism test and mechanical property test of concrete were prepared in accordance with GB/T 50082-2009 [29] and GB/T 50081-2009 [30]. The water/cement ratio applied to all the mixtures was 0.42. For all specimens, the fine

Table 1: Physical and mechanical properties of P·O 42.5 cement

Indexes	Standard consistency (%)	Fineness ($cm^2 \cdot g^{-1}$)	Stability	Setting time (min)		Flexural and compressive strength (MPa)	
				Initial setting	Final setting	3 days	28 days
Results	27.5	3830	Qualified	134	224	5.2/34.7	8.3/49.6

Table 2: Chemical compositions of cement (%)

Oxides	Na_2O	K_2O	MgO	CaO	SiO_2	Al_2O_3	Fe_2O_3	Loss on ignition
w (%)	0.42	0.72	2.32	59.06	28.60	8.11	3.72	0.60

Table 3: Chemical compositions of quartz sand (%)

Oxides	MgO	CaO	SiO_2	Al_2O_3	Fe_2O_3
w (%)	0.080	0.035	99.55	0.14	0.19

aggregates (natural medium sand) were partially replaced by 3 and 6% by mass of the reactive aggregates, which were denoted as CLA-4 and CHA-4, respectively, and the mixture proportions are shown in Table 4. The concrete specimens were mixed according to the components in Table 4 and removed from the mold after forming, and the specimens were maintained in a standard curing room at 40°C with a relative humidity of 100 to the specified ages.

2.3 Test methods

2.3.1 ER of concrete prisms test

The concrete prism test was carried out on the specimens following the standard of GB/T 50082-2009 [29]. The concrete prism specimens measured 75 mm × 75 mm × 275 mm in size, with three specimens per group. The age was extended to 245 days to observe the later ER. The changes in length and mass were measured using a digital length comparator and scale, respectively.

2.3.2 Mechanical property tests

The ACS and STS experiments of concrete specimens were measured according to GB/T 50081-2019 [30], and the RDEM test of concrete specimens was performed in accordance with the National Standards of China GB/T 50082-2009 [29]. The dimensions of the ACS, STS, and RDEM of concrete specimens were 150 mm × 150 mm × 300 mm, 100 mm × 100 mm × 100 mm, and 100 mm × 100 mm × 400 mm, respectively. Besides, the ACS, STS, and RDEM of concrete specimens were measured at different curing ages.

2.3.3 XRD analysis

To characterize the phase changes of the reaction products within 35 weeks, the XRD measurements were taken using an XRD (Bruker D8 Advance, Germany). The step size and scanning rate of this apparatus were 0.02° and $5° \cdot min^{-1}$, respectively. The specimens were scanned in the range from 10° to 90°.

2.3.4 SEM/EDS test

To explore the effect of ASR on the microstructure of concrete, the microstructural characteristics of samples at different ages, including the changes in the microstructure

Table 4: Mixture proportions of concrete specimens ($kg \cdot m^{-3}$)

Types	Cement	Fine aggregate	Quartz sand	Coarse aggregate	Water	10% NaOH solution
CHA-4	420	714.4	45.6	1140	176	14.96
CLA-4	420	737.2	22.8	1140	176	14.96

Notes: CHA-4 referred to concrete specimens with 6% dosage reactive aggregate; CLA-4 represented concrete specimens with 3% content reactive aggregate.

morphology and chemical component of hydration products, were studied. The samples were examined using a thermal field emission scanning electron microscope and an energy-dispersive X-ray spectrometer and the specimens were scanned using an apparatus mode with a voltage of 15 kV and a current of 4 MPa.

2.3.5 X-ray CT test

X-ray CT was applied to observe the variation in porosity and the progression of ASR influence over 35 weeks. The specimens used for X-ray CT were thin slices of concrete with a diameter of 18 mm and a height of 6 mm. And the slices were randomly chosen for observational purposes.

The 3D computed tomography microscanning system primarily consists of an X-ray source, rotating sample stage, detector, and computer system. X-ray CT measures the topography of the sample alone and reconstructs it to obtain a three-dimensional image. During this process, the X-ray intensity will attenuate due to the absorption or scattering of the sample, and its intensity reduction complies with the Lambert–Beer law [31]. The composition of the microcomputed tomographic system is shown in Figure 3.

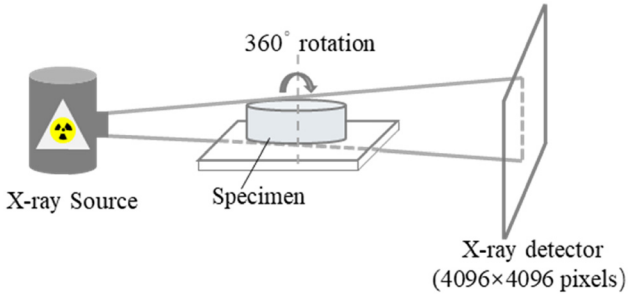

Figure 3: Schematic diagram of the X-ray CT.

3 Results and discussions

3.1 ER of concrete prisms

Figure 4 presents the ER changes of concrete prisms containing 3 and 6% reactive aggregate. As can be seen from Figure 4(a), the ERs of all tested samples far exceeded the limits specified (0.04%) in ASTM C1260 [32] and SL 352–2020 [27], and the ER of the CHA-4 group was significantly larger than that of the CLA-4 group.

For the trend of ER versus time, the hyperbolic function of Liu was used to fit [33], and the fitted curve and related parameters are detailed in Figure 4(b) and Table 5, respectively, and the equation of the hyperbolic function is shown in Eq. (1). As can be seen from Table 5, the correlation coefficient R^2 values of the CHA-4 and CLA-4 groups are equal to 0.9906 and 0.9953, respectively, and their values are close to 1, so the hyperbolic function provides an excellent fit. At the same time, the relationship between the ER and time was fitted to derive the reaction rate (k_T) and the final ER (ξ_u) by Origin in order to further analyze the expansion trend of concrete prisms.

$$\xi_2(t) = \frac{\xi_u k_T t}{1 + k_T t}, \tag{1}$$

where $\xi_2(t)$ and ξ_u are the expansions of concrete prisms at the curing time of t and the final ERs, respectively. And k_T and t are the reaction rate constant at T°C and the curing time of the specimens at T°C, respectively.

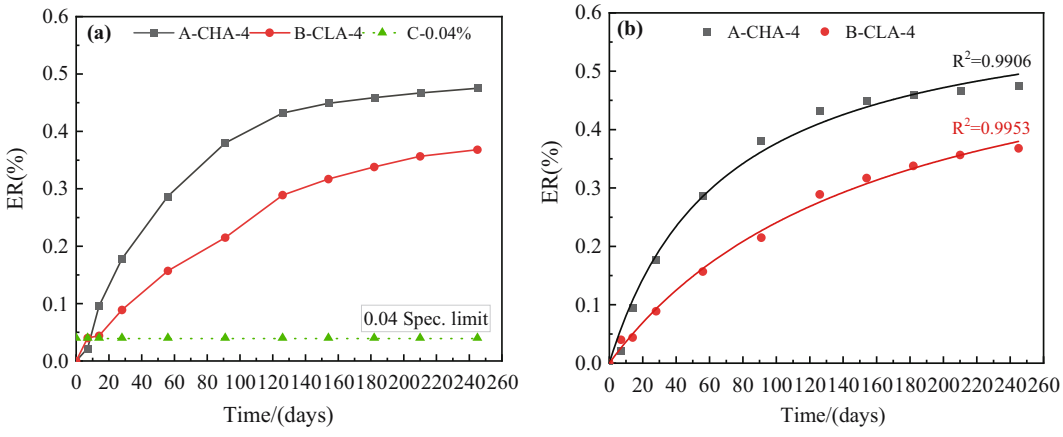

Figure 4: Relationship between the ER and curing age of the CHA-4 and CLA-4 group concrete specimens: (a) ER and (b) fitting curve of the ER of CHA-4 and CLA-4 groups.

Table 5: Regression parameters of the fitting curve about the relationship between expansion and time of CHA-4 and CLA-4 groups

Types	ξ_u (%)	k_T (d^{-1})	R^2
CHA-4	0.6319	0.0147	0.9906
CLA-4	0.6310	0.0062	0.9953

Combined with the analysis of the ER data obtained from the test, the difference between the ER growth of the CHA-4 and CLA-4 groups in the two time periods of 56–91 days and 91–126 days was large, which demonstrated that the growth rate of the ER of both changed at 91 days, and the reaction rate of the prisms at the corresponding time point could be calculated by Equation (1). The reaction rates of the CHA-4 group specimens were 0.0158, 0.0145, and 0.009 at 56, 91, and 126 days, respectively, while the reaction rates of the CLA-4 group specimens were recorded as 0.006 and 0.0056 at 56 and 91 days, respectively. The reaction rates of the CHA-4 and CLA-4 groups gradually leveled off around 126 and 91 days, respectively. Meanwhile, in conjunction with the analysis of Figure 4, the reaction rates of CHA-4 and CLA-4 gradually stabilized around 126 and 91 days, respectively.

The ER results demonstrated that all the two groups of concrete prisms containing 3 and 6% reactive aggregates showed a sharp increase in expansion at an early age, while concrete prisms' ER in the later stage entered a stable stage until the end of the observation period, which indicated that the ASR process entered the end stage.

3.2 Variation of weight gain rate with time

Figure 5 illustrates the evolution of weight gain in concrete prisms of the CHA-4 and CLA-4 groups with the increase in curing age. It could be seen from Figure 5 that the weights of CHA-4 and CLA-4 increased continuously with the growth of maintenance age, and the weight gain rate of the CHA-4 group was greater than that of the CLA-4 group. The weight gain rate of the two groups both reached a maximum value of 1.2 and 0.6%, respectively, at 126 days, while the weight gain rate of the two groups both exhibited a sharp decline in the segment after 126 days. And with the progress of the experiment, the weight gain rate of the concrete prism became negative in the later periods. It could be concluded that as the ASR took place, the prism masses of both high and low dosing reactive aggregates demonstrated a tendency that increased first and then decreased. On the one hand, the weight gain rate gradually

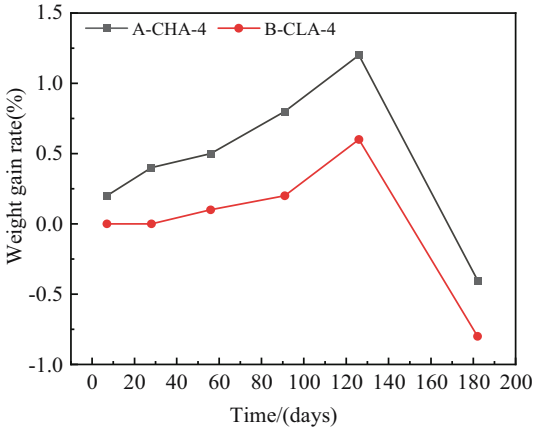

Figure 5: Weight gain rate of the CHA-4 and CLA-4 group concrete prisms.

became larger as the age increased. On the other hand, the higher the dosage of reactive aggregates was, the greater the weight gain rate of the concrete prism would be.

This tendency was caused by the internal expansion of concrete prisms brought on by the ASR gel's water absorption, which increased the weight of concrete prisms [15,34]. The growing gel pockets in the aggregates would create expansion pressure inside the concrete, and the internal stress accumulated to a high level that the concrete could no longer support, resulting in a growing number of cracks in the prisms. The evolution of cracks would lead to an increase in the permeability and water absorption rate of concrete prisms, thus increasing the weight gain rate of concrete prisms [35]. The concrete prisms containing 6% reactive aggregates would have more ASR gel accumulation, resulting in more cracks and a greater weight gain rate. Due to the increasing number of cracks and extension width, the concrete aggregates were forced apart from the matrix, which ultimately led to the appearance of a sharp decrease segment in the weight gain rate. The results also indirectly indicated that the internal structures of the CHA-4 and CLA-4 groups were damaged to different degrees with the increase of curing age. Furthermore, the internal damage was constant and the mechanical properties became worse in the process of the mass increase.

3.3 Analysis of the ACS

The variations of ACS with the increase of curing age for the investigated CHA-4 and CLA-4 group concrete prisms are illustrated in Figure 6. It can be obtained from the picture that under the influence of ASR, the overall ACS of all concrete prisms showed a continuous downward

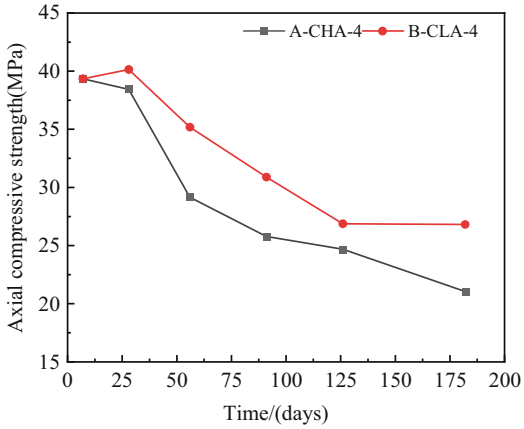

Figure 6: Relationship between the ACS and curing age of the CHA-4 and CLA-4 groups.

trend. The CHA-4 group, on the other hand, similarly exhibited a reduced declining rate of the curve during the period from 7 to 28 days, while the CLA-4 group displayed a minor growing segment of strength for the first 28 days. This trend could be due to the strong initial hydration of cement, which weakened the damage caused by ASR to the ACS [18]. During the period from 28 to 126 days, the decline rate of the ACS of the CHA-4 group was greater than that of the CLA-4 group in the early period. The decline rate of the ACS of the CLA-4 group tended to be stable in the latter stage, and the decline rate of the ACS of the CHA-4 group appeared to slow down. At 126 days, the ACS of the CLA-4 group had decreased to a minimum value of 28 MPa, whereas the ACS of the CHA-4 group had not yet stopped declining. The results demonstrated that with the increase in curing time, the ACS of concrete prisms was weakened by ASR. The higher the dosage of reactive aggregates was, the greater the weakening effect of ASR on the ACS of concrete would be. Meanwhile, the ACS might be affected by the interactive effect of the hydration reaction of the cement and ASR in the early stage of the experiment, which indicated that the evolution of the ACS might mask the damage caused by ASR in the early stage.

It is worth mentioning that the hydration reactions of the cement as well as the ASR-related degradation have an impact on the mechanical characteristics of concrete. The former diminished the mechanical properties of concrete, while the latter enhanced these properties [18]. For the CLA-4 group concrete prisms, at the start of the experiment, the hydro-chemical reaction of cement dominated. The strength increase brought on by the cement's ongoing hydration was stronger than the influence of ASR-induced damage on the mechanical properties of concrete. Similarly, for the CHA-4 group concrete prisms, the hydro-chemical reaction of cement also lessened the harm that ASR had done to the stiffness and compressive strength of concrete. The ACS declined at a slower rate throughout the first 28 days as a result. After 28 days, the negative effect of ASR on the ACS grew more pronounced, and even though the hydration reactions of the cement continued, the adverse effect from ASR-induced damage on the ACS still dominated. Therefore, the ACS showed a downward trend in the later stage. This indicated that the 28-day ACS of concrete prisms containing reactive aggregates could not effectively reflect the degradation of ASR mechanical properties, which should be paid attention to in practical engineering applications.

3.4 Analysis of the STS

The impact of ASR on the tensile behavior of the concrete can be best reflected by the splitting test. Figure 7 shows the variation of STS of concrete prisms with the increase in curing age. It can be seen in the figure that the STS reached a maximum value for both concrete prisms with various reactive aggregate dosages before it started to reduce. The maximum value of the STS of the CHA-4 and CLA-4 groups was 3.4 and 3.7 MPa, respectively. The stronger ASR caused the CHA-4 groups to reach their maximum values at 28 days, whereas the weaker ASR caused the CLA-4 groups to reach their highest values at 56 days. After reaching the maximum value, a significant decline in strength was seen in both the CHA-4 and CLA-4 groups, followed by a gentle section. At 56 days, the CHA-4 groups decreased to 1.6 MPa, while the CLA-4 groups dropped to 2.2 MPa at 91 days. The findings demonstrated that the STS of the concrete prisms with various reactive aggregate dosages

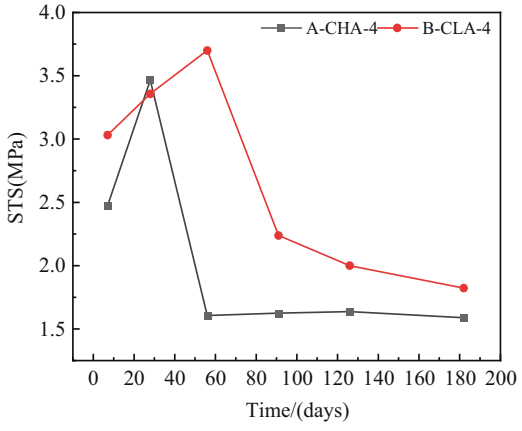

Figure 7: Relationship between the STS and curing age of the CHA-4 and CLA-4 groups.

tended to increase strength in the early stages and decrease strength in the late stages. The reason was that in the initial stage, the continual hydration of cement and the gel's ability to plug in the cracks improved the microstructure of concrete, which temporarily raised the STS [15,24]. And the more the reactive aggregate was, the shorter the enhancement stage would be. With the progression of ASR in concrete, the existing microcracks might extend into the matrix and form a network, which connected the microcracks proceeding through the reactive aggregate. The microcracks also kept increasing continuously in number, length, and width. The matrix was eventually not sufficient to resist the damage caused by ASR, and the STS appeared to decrease sharply.

3.5 Analysis of the RDEM

Due to its high sensitivity to microcracks and aggregate grading, the RDEM is acknowledged as a useful index to demonstrate the negative consequences of ASR [14,23,36–40]. Figure 8 is plotted to clarify the variation of the RDEM of the concrete prisms with the increase in curing age. It can be seen from Figure 8(a) that the RDEM of the CHA-4 and CLA-4 groups displayed a consistent tendency toward decline, with both of them showing the fastest fall rates before 56 days. At the same time, the RDEM has been in the lowering stage throughout the observation period, and the decline rates of the RDEM of the CHA-4 and CLA-4 groups were comparable at a later stage. The curve-fitting results between the RDEM and time are represented in Figure 8(b); it could be concluded that the degradation of RDEM of concrete was well described by the fitting curve, and the R^2 values in the CHA-4 and CLA-4 groups reached 0.99 and 0.95, respectively. This also indirectly indicated that the RDEM was much more sensitive to the progression of cracks with the increase of curing age. The investigation revealed that the concrete's RDEM was a reliable predictor of the negative effects of ASR (*i.e.*, expansion), that it declined over time, and that the amount of reactive aggregate in the later phases had a minimal bearing on the reduction of it. Though the RDEM of concrete was still in the declining stage, the accuracy of the dynamic elastic modulus detection dropped as a result of more damage inside the prisms at a later stage. Though the RDEM of concrete was still in the declining stage, the RDEM could still effectively describe the internal damage of ASR. This revealed that the concrete's RDEM was a reliable predictor of the negative effects of ASR (*i.e.*, internal damage).

4 Establishment of the failure criteria

4.1 Analysis of the relationship between the limits of each parameter

It can be seen from the aforementioned analysis that the RDEM was the most accurate index for indicating the extent of ASR damage. Combined with the ER, the weight gain rate, the relative ACS, and the relative STS, the RDEM was chosen as the reference group for comparative analysis in this study.

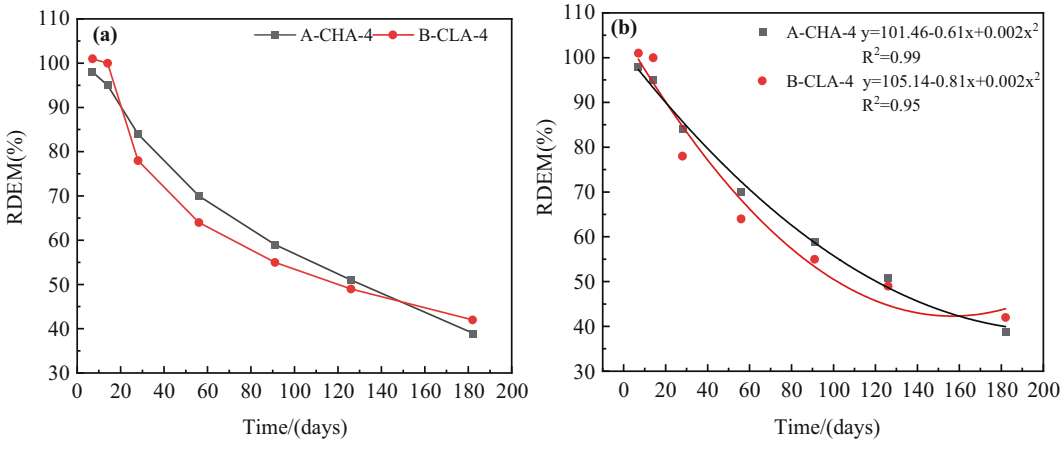

Figure 8: RDEM and fitting curve between the RDEM and curing age of the CHA-4 and CLA-4 groups: (a) RDEM of the CHA-4 and CLA-4 groups and (b) fitting curve of the CHA-4 and CLA-4 groups.

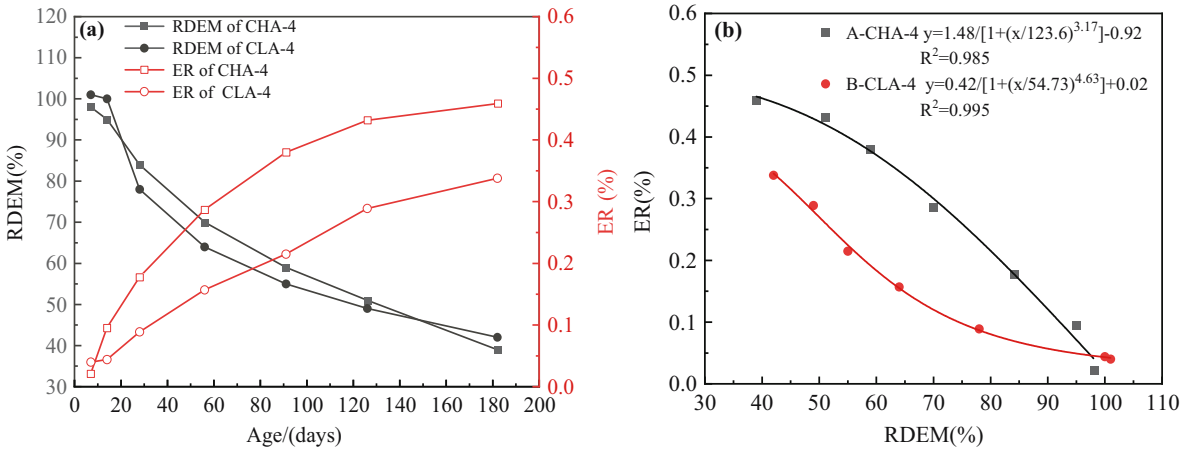

Figure 9: Relationship between the RDEM and the ER: (a) relationship between the RDEM and the ER with curing age and (b) the fitting curve of the RDEM and the ER.

4.1.1 Relationship between the RDEM and ER

Both the relationship between the RDEM and ER with ages and the fitting curve of the RDEM and expansion were plotted for concrete prisms, as shown in Figure 9. From Figure 9(b), the CHA-4 and CLA-4 groups' RDEM and ER fitting curves obtained values of the regression coefficient (R^2) of 0.985 and 0.995, indicating a very good fitting relationship between the RDEM and ER. Consequently, there was a close connection between the RDEM and the ER. As ASR progressed inside the concrete, the ER of concrete prisms continuously increased, while the RDEM of concrete prisms gradually decreased. Therefore, according to the RDEM of the concrete prisms undergoing an internal damage limit state, the growth limits of the ER could be further determined.

Based on extensive tests, Swamy [22] found that when the first crack generated by ASR appeared on the concrete surface, the corresponding ERs ranged from 450 to 650 $\mu\varepsilon$, that is, 0.045–0.065%. It can be observed from Figure 9 that the ER of the concrete prisms in this study was already in the range of 0.045–0.065% at the early stage, in which the first crack was generated. However, the lack of a clear loss of mechanical qualities at this range suggested that the first crack's formation had little effect on the mechanical properties of the concrete.

Figure 10 exhibits the gels and cracks on the surface of the CHA-4 and CLA-4 prisms when the RDEM was reduced to 70 and 60%, respectively. Following the observations in this study, when the RDEM of the CHA-4 group either decreased to 70% and the ER was 0.287%, or the RDEM of the CLA-4 group decreased to 60% and the ER was 0.182%, the cracks on the specimen's surface increased sharply and numerous gels appeared subsequently, indicating that the ER of concrete had reached the limit values at this time. In conclusion, the limit values of ER for the CHA-4 and the CLA-4 groups are when the RDEM decreases to 70 and 60%, respectively.

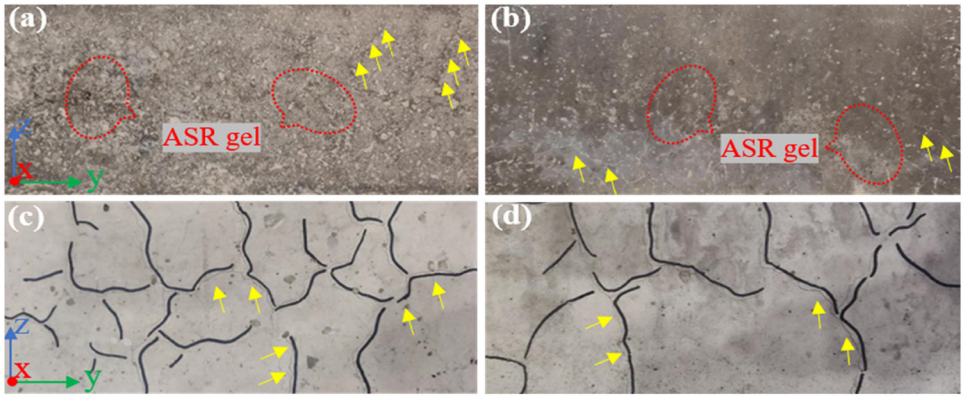

Figure 10: Gels and cracks on the surface of the concrete prisms: (a) gels of the CHA-4 group when the RDEM was 70%; (b) gels of the CLA-4 group when the RDEM was 70%; (c) cracks of the CHA-4 group when the RDEM was 70%; and (d) cracks of the CLA-4 group when the RDEM was 60%.

Figure 10 exhibits the gels and cracks on the surface of the CHA-4 and CLA-4 prisms. Liu *et al.* [21] found that when the corresponding RDEM was 83.34%, large cracks appeared on the surface of concrete accompanied by visible gel overflow. When the RDEM of the CHA-4 and CLA-4 groups fell to 70 and 60% in this study, respectively, large cracks appeared on the surface of the specimen and gel overflow occurred (Figure 10). At this point, the mechanical properties decreased significantly.

Following the observations in this study, when the RDEM of the CHA-4 group either decreased to 70% and the ER was 0.287%, or the RDEM of the CLA-4 group decreased to 60% and the ER was 0.182%, the cracks on the specimen's surface increased sharply and numerous gels appeared subsequently, indicating that the internal damage of concrete was very serious at this time, and the mechanical properties deteriorated obviously (Figures 6 and 7), which was no longer suitable for continuous load bearing. In conclusion, the limit values of ER for the CHA-4 and the CLA-4 groups are when the RDEM decreases to 70 and 60%, respectively.

4.1.2 Relationship between the RDEM and the relative ACS with time

According to GB/T 50476-2019 [41], the concrete structure should meet the reliability requirements of the serviceability limit state, the reliability of concrete should be 90–95%, and the corresponding failure probability should be 10–5%. For the percentage loss of the relative ACS of concrete, the variations between RDEM and the relative ACS with time in this study are shown in Figure 11. It could be concluded from Figure 11 that the RDEM of the CHA-4 group reduced to 82.25 and 79.33% under the influence of ASR when the relative ACS was lost by 5 and 10%, while the RDEM of the CLA-4 group decreased to 69.38 and 64%. The findings revealed that the RDEM reduced to 69.38 and 64% when the relative ACS of the low dosage of reactive aggregates reached the loss limit and to 82.25 and 79.33% when the relative ACS of the high content of reactive aggregates reached the loss limit.

4.1.3 Relationship between the RDEM and the relative STS with time

According to the previous analysis, before the weakened point of the STS, there would be a temporary strengthening phase of the STS for a certain period due to the bonding effect of the gel. However, the subsequent decline section belongs to the brittle failure stage, and brittle failure is strictly prohibited in concrete structures. Therefore, the loss limit of the STS should be determined before the decline stage, that is, the peak point. Figure 12 is plotted to clarify the influence of expansion due to ASR on the RDEM and the relative STS over time. As can be seen from Figure 12, the RDEM must be reduced to 84% for the loss limit of STS of high content reactive aggregate specimens (CHA-4), while the RDEM must be reduced to 64% for the loss limit of STS of low content active aggregate specimens (CLA-4).

4.1.4 Relationship between the RDEM and the weight gain rate with time

The trends of RDEM and the weight gain rate with curing age throughout the period investigated are depicted in

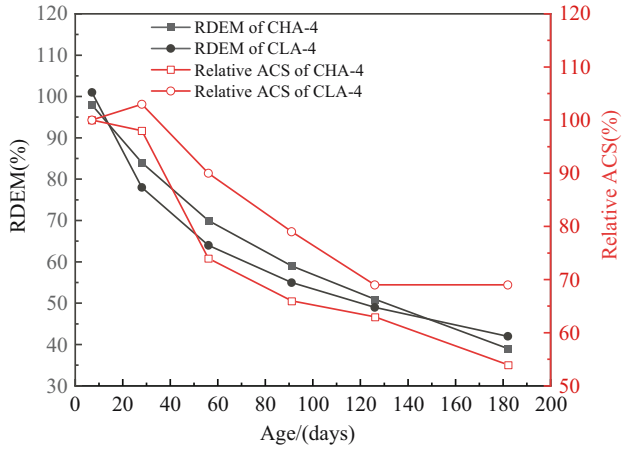

Figure 11: Relationship between the RDEM and the relative ACS with curing age of the CHA-4 and CLA-4 groups.

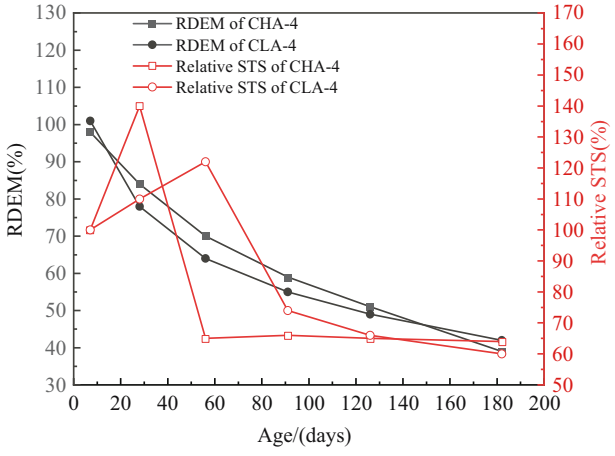

Figure 12: Relationship between the RDEM and the relative STS with curing age of the CHA-4 and CLA-4 groups.

Figure 13. From Figure 13, it can be observed that as the RDEM was continuously reduced, the weight gain rate abruptly decreased after reaching its maximum value. At the same time, the RDEM of the high-dosage (CHA-4) and low-dosage (CLA-4) reactive aggregates corresponded to 51 and 49%, respectively, when the weight gain rate of the CHA-4 and CLA-4 groups reached the maximum values. Besides, combined with Figures 11 and 12, when the RDEM of the CHA-4 and CLA-4 groups were 51 and 49%, respectively, the corresponding relative ACS and relative STS were reduced to 62, 75%, and 64, 72%, respectively. These results indicated that the specimens had lost their bearing capacity and the concrete had sustained serious damage at this point; thus, the weight gain rate was not a reliable indicator of characterizing the extent of the damage inside the concrete.

4.2 Determination of the failure criteria

4.2.1 Influence of dosages of reactive aggregate on mechanical properties

Combined with the analysis of Figures 9 and 11 and and 12, it can be obtained that the ERs were 0.089, 0.17, and 0.215 for the CLA-4 group when the ages were 28, 60, and 91 days, respectively, while the ACS increased by 2% at 28 days, decreased by 12% at 60 days, and reduced by 21% at 91 days. The STS at 28 and 60 days increased by 11 and 15%, respectively. The STS decreased by 26% at 91 days. The RDEM was 78, 66, and 55% at 28, 60, and 91 days, respectively; when the ages were 28, 60, and 91 days, the ERs were 0.178, 0.296, and 0.38 for the CHA-4 group, respectively, while the ACS decreased by 4, 27, and 34% at 28, 60, and 91 days, respectively. The STS increased by 38% at 28 days, decreased by 34% at 60 days, and reduced by 33% at 91 days, and the RDEM at 28, 60, and 91 days was 84, 70.4, and 59%, respectively.

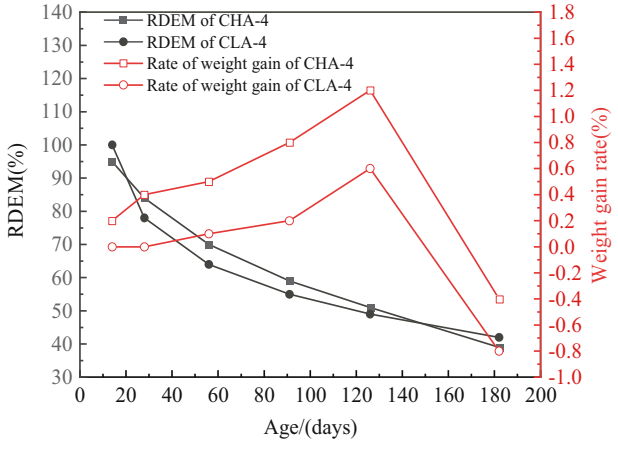

Figure 13: Relationship between the RDEM and the weight gain rate with curing age of CHA-4 and CLA-4 groups.

By comparing the results, it was discovered that the amount of reactive aggregate in concrete has a significant impact on its mechanical properties. The more reactive aggregate there is, the more seriously the concrete is damaged internally and the less bearing capacity the specimens have at the same age. In addition, it was observed that when the content of reactive aggregate was higher under the same damage degree, the degradation age of the mechanical properties would be earlier. It is noteworthy that the degradation age of mechanical properties of the CLA-4 groups has not reached and the ASR had little impact on the mechanical characteristics of the concrete when the RDEM was approximately 80%, whereas the degradation age of the mechanical properties of the CHA-4 groups reached and the bearing capacity decreased (Figures 11 and 12). Therefore, it could be inferred that the RDEM had the ability to accurately characterize the interior concrete damage to a greater extent with a higher dosage of reactive aggregates.

4.2.2 Determination of the scopes of the failure criteria

The limit values of the RDEM for each parameter under the influence of ASR are summarized in Table 6. Following a horizontal comparison, it was discovered that the limit values for the weight increase rate and ER of the CHA-4 group were lower than the limit values for the relative ACS and the relative STS. As a result, the failure criterion of the CHA-4 group was developed based on the limit values of the relative ACS and the relative STS. The concrete structure was close to its maximum load-bearing capacity when the RDEM was reduced to 84%, the STS achieved its maximum value, and the ACS lost almost 5%. At this point, the brittle failure stage had not yet been reached. Therefore,

Table 6: RDEM corresponding to each parameter limit value

Types	E_{r1} (%)	E_{r2} (%)	E_{r3} (%)	E_{r4} (%)
CHA-4	82.25	84	70	51
CLA-4	69.38	64	60	49

Note: E_{r1} refers to the corresponding RDEM when the relative ASC reached the limit value; E_{r2} denotes the corresponding RDEM when the relative STS achieved the limit value; E_{r3} represents the corresponding RDEM when the ER is up to the limit value; E_{r4} implies the corresponding RDEM when the weight gain rate was at its limit value.

the ASR failure criterion for the CHA-4 group would be adopted as a decrease in the RDEM to 84%.

In comparison with the limiting values of ER, the relative ACS, and the relative STS, the limiting values of weight gain rate for the CLA-4 group were much lower. Therefore, the ER, relative ACS, and relative STS limiting values would be used to define the failure criterion for the CLA-4 group. The STS was prevented from reaching its maximum value and from moving on to the brittle failure stage when the RDEM was lowered to 69.38%, while the ACS lost 5% and the ER was prevented from reaching its limiting value. Therefore, a decrease in RDEM to 69.38% was considered as the ASR failure criterion for the CLA-4 group.

In summary, the failure criteria of ASR for the CHA-4 and CLA-4 groups were a decrease in the RDEM to 84 and 69.38%, respectively, taking values of 85 and 70%. The failure criteria of ASR should be treated as a greater value than the test value in practical engineering due to the complicated aspects of the material and maintenance environment and on account of safety reserve, and the limit range should be extended by 5%. For the CLA-4 group of concrete at 40°C, the RDEM decrease range of 70–75% is chosen as the ASR failure threshold; the RDEM decrease range of 85–90% is taken as the ASR failure criterion for the CHA-4 group of concrete at 40°C.

5 Microstructure analysis

5.1 Analysis of XRD

To investigate the variation of phase types of the concrete prisms after being cured for 14, 56, 126, and 245 days, the samples were examined using the XRD technique. The severe reaction led to the selection of the CHA-4 group sample for XRD examination of the corresponding periods. The XRD spectrum of the CHA-4 group is shown in Figure 14. It was found from Figure 14 that the types of the physical phases include SiO_2 and C_2S and C_3S, in addition to the products of hydro-chemical reaction of cement such as $Ca(OH)_2$, C-S-H gel, calcium alumina, and $CaCO_3$. In addition, the plots of the samples at different ages were compared, and it could be seen that only the height and intensity of characteristic peaks changed. With the evolution of age, the number of $Ca(OH)_2$, $CaCO_3$, AFt, and C-S-H gel gradually increased, while the number of C_2S and C_3S decreased gradually. Therefore, during the observation period, the phase type did not change, but only the amount of the corresponding substance changed.

5.2 Analysis of SEM/EDS

Next, SEM was used to observe the microscopic morphology of the sample CHA-4 at the corresponding age; the outcomes are depicted in Figures 15 and 16. EDS analysis of the hydro-chemical products at points 1–2 in Figure 16 revealed that the component elements are mainly Ca, Na, Si, and K. In conjunction with related researches, it was indicated that ASR gels at the hit points in the specimens were all ASR products [7,42–44], and their EDS profiles are shown in Figure 17, and the chemical composition is shown in Table 7.

Figure 15(a) and (c), (b) and (d) are the SEM images of the CHA-4 group and the CLA-4 group after curing for 56 and 126 days, respectively. It could be seen by comparing

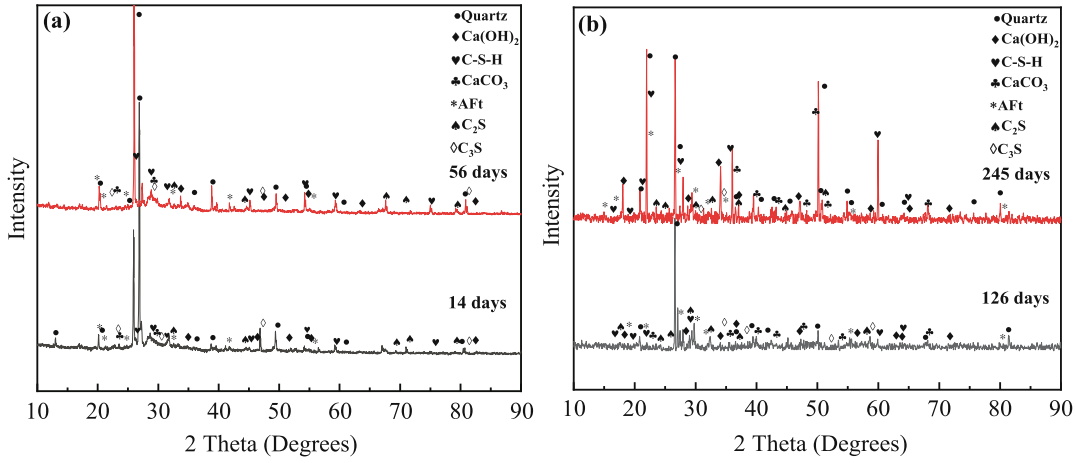

Figure 14: XRD of the samples of the CHA-4 group: (a) cured for 14 days, (b) cured for 56 days, (c) cured for 126 days, and (d) cured for 245 days.

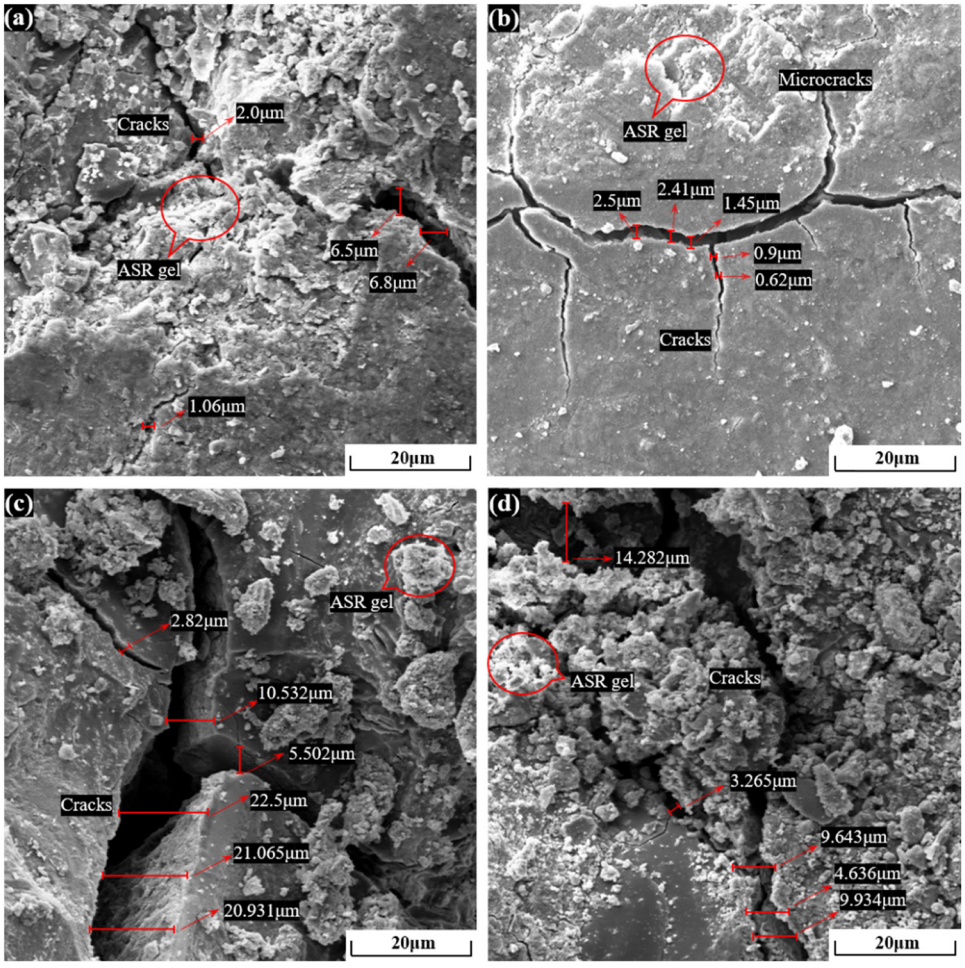

Figure 15: Microscopic observations of the CHA-4 and CLA-4 groups: (a) and (b) cured for 56 days and (c) and (d) cured for 126 days.

Figure 15(a) and (c), (b) and (d) that the crack width gradually increased with the evolution of the process of ASR, and the cracks were filled with a large amount of ASR gels; it was evident through observing Figure 15(a) and (b), (c) and (d) that the width and number of cracks of the prisms in the CHA-4 group were higher than those in the CLA-4 group at 56 and 126 days, indicating that the damage degree caused by ASR was greater than that of the prisms in the CLA-4 group as the curing age increased. It was determined that prisms with a high dosage of reactive aggregates had more ASR damage than prisms with a low dosage of reactive aggregates as the ASR developed. Additionally, for concrete of the same age, interior damage to the material increases with reactive aggregate dosage.

At 56 days, the ACS of the CHA-4 and CLA-4 groups decreased by 25.9 and 10.5%, respectively, while the STS of CHA-4 and CLA-4 groups decreased by 35% and increased by 22%, respectively. Combined with SEM, the mechanical properties of concrete prisms were significantly reduced, which was consistent with the previous analysis of mechanical properties. In addition, the damage caused by ASR had little effect on the STS of the CLA-4 group for 56 days. Furthermore, the damage caused by the microcracks of ASR had less influence on the STS than that of ACS. At the same time, the cracks continue to expand, which will significantly reduce the mechanical properties of concrete.

The electron micrographs of the concrete prism of the CHA-4 group maintained for 7, 56 and 126 days are shown in Figure 16. It was found from Figure 16(a) that there were only a few C-S-H gels on the surface of the reactive aggregates at the age of 7 days, but with the increase of curing age, the hydration products of C-S-H increased quickly, which can be observed from Figure 16(b)–(d). It is revealed that the ASR gel was primarily formed inside the cement paste matrix and at the interface between the glass aggregate and the cement paste. Besides, the samples' hydration products were rather dense, and many needle-like calcium alumina crystals were formed on the surface of the aggregate after curing for 56 days (Figure 16(c)) and 126 days (Figure 16(d)). Additionally, the continuous flocculent ASR

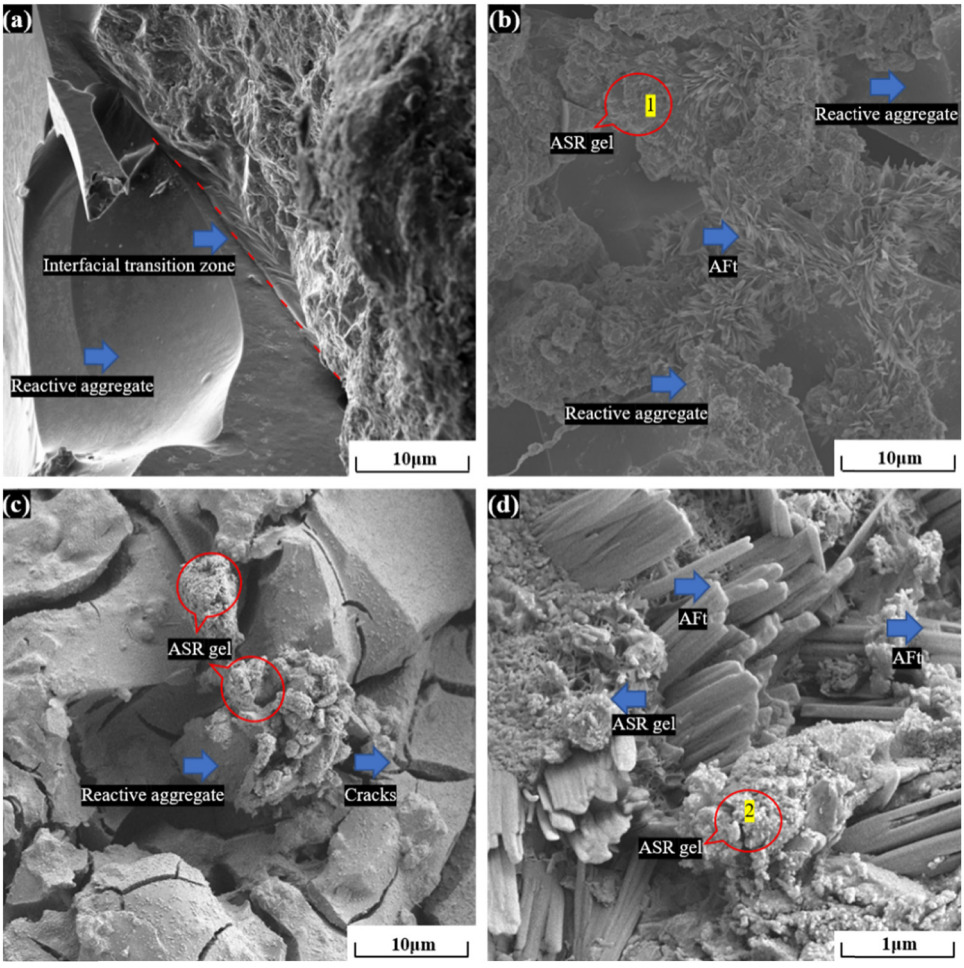

Figure 16: Microscopic observations of the CHA-4 group: (a) cured for 7 days, (b) cured for 56 days, and (c) and (d) cured for 126 days.

gels were entangled with one another. From the SEM inspection, it was revealed that with increasing curing time, the harmful manifestations inside the matrix increased, and the colorless and transparent flocculent ASR gel gradually overflowed to the outer region, producing many irregularities and parallel-oriented cracks.

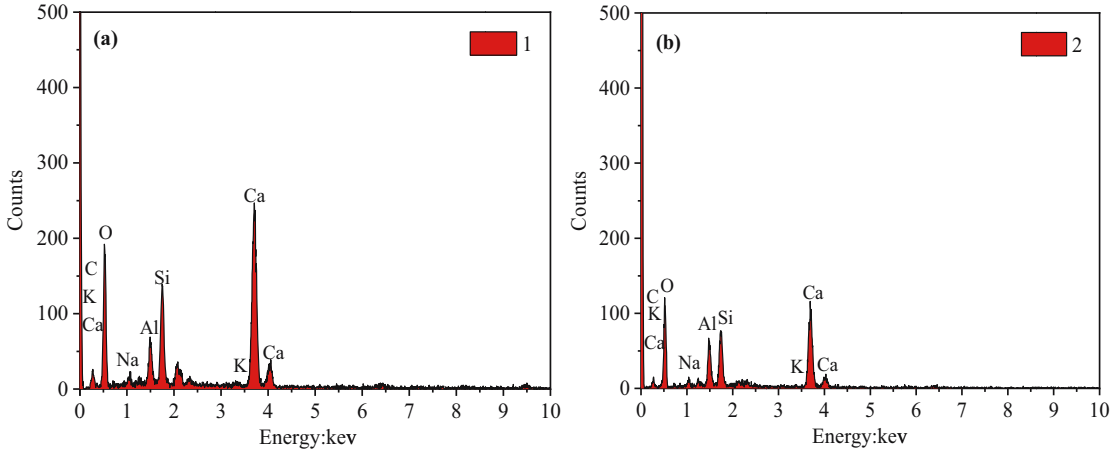

Figure 17: EDS analysis of the CHA-4 group after curing for 56 and 126 days: (a) CHA-4 cured for 56 days and (b) CHA-4 cured for 126 days;.

Table 7: EDS data (by weight) of hydration products (%)

Types	Na	Al	Si	K	Ca	C	O	Ca/Si	Na/K
CHA-4 56 days	0.53	3.19	5.51	0.23	24.26	5.41	60.88	4.4	2.3
CHA-4 126 days	1.32	6.16	8.8	0.34	26.93	5.35	51.1	3.06	3.88

5.3 Analysis of X-ray CT

5.3.1 Microstructural investigation of ASR gel damage

To investigate the ASR damage of reactive aggregates and the crack propagation in aggregates, X-ray CT scanning was carried out on the specimens. Figures 18 and 19 are the two-dimensional cross-sectional and longitudinal tomography images of the CHA-4 group at 7, 56, and 126 days, respectively. Besides, the darkest zones denote pores, the little-bit of darker gray zones are aggregates, and the lighter zones are the slurry of cement.

It can be seen from Figures 18(a) and 19(a) that the aggregate surface was smooth and complete, and there were no microcracks after the sample had been curing for 7 days. Besides, there were initial defects on the surface of some glass aggregates. Early in the reaction, the reactive aggregates were not dissolved or altered because the matrix structure was compact and there was little contact between the alkali and the reactive aggregates. At this time, combined with the analysis of Figures 6 and 7, it was found that the ACS and STS of the concrete prism were in the growth stage, and ASR has less damage to the mechanical properties of the concrete prism at the early age.

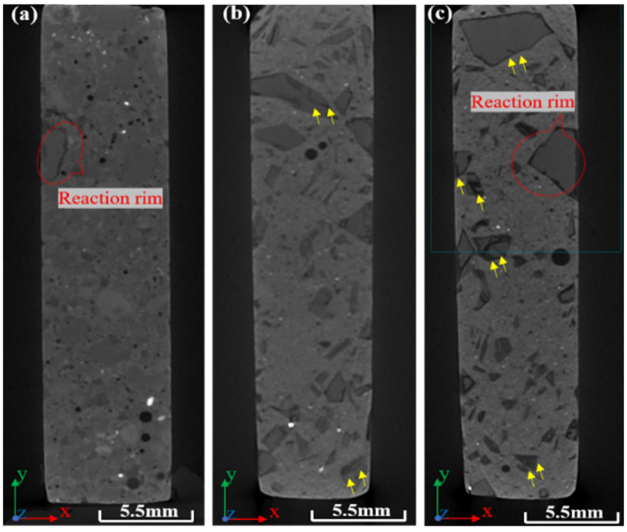

Figure 19: Two-dimensional longitudinal-section pictures of the CHA-4 group: (a) cured for 7 days, (b) cured for 56 days, and (c) cured for 126 days.

Then, when the specimen was up to the age of 56 days, the aggregate microcracks progressively occurred on the surface, and a ring-shaped fracture on the surface of the aggregate induced by ASR gel pressure was also observed. And a pale reactive ring was observed in the surroundings of the aggregates, the aggregates were in part dissolved, and the surface of the glassy aggregates progressively turned coarse and cracked. In addition, as the maintenance age increased, the gel filled the voids, the color of the defective reactive aggregate was darker [45,], and the shape of the pores progressively turned to be a state of irregularity. At this time, the ACS and the STS of the CHA-4 group of the prism were in the declining stage. Therefore, when combined with Figure 15, it could be seen that the crack widths

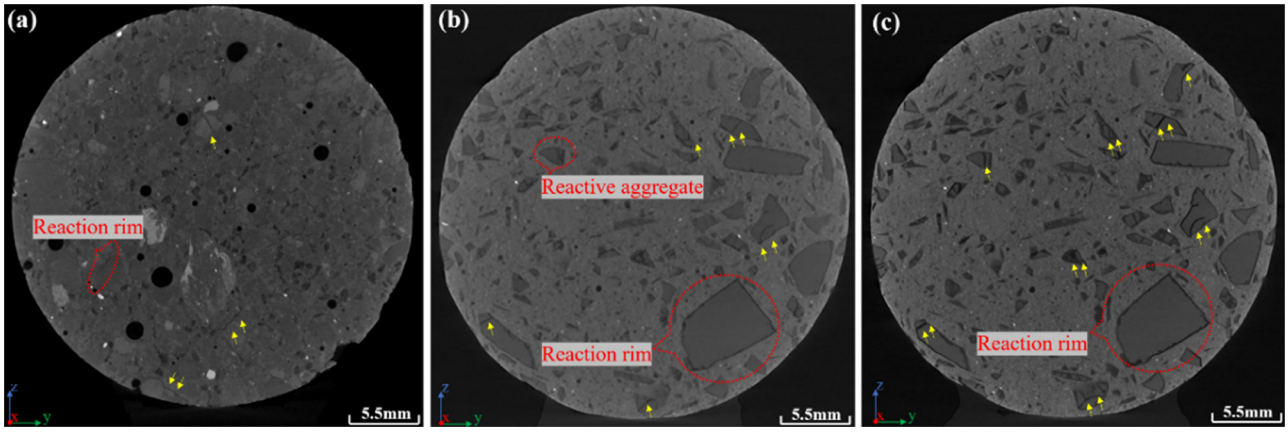

Figure 18: Two-dimensional cross-sectional pictures of the CHA-4 group: (a) cured for 7 days, (b) cured for 56 days, and (c) cured for 126 days (the arrows emphasize the cracks in the mortar samples).

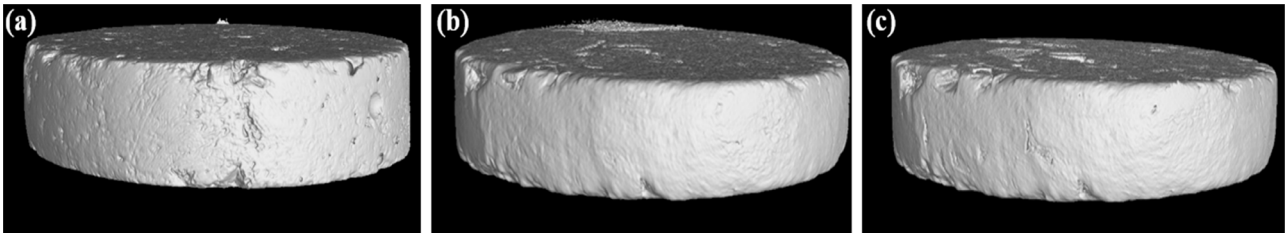

Figure 20: Three-dimensional original images of the CHA-4 group obtained from tomographic data: (a) CHA-4 for 7 days, (b) CHA-4 for 56 days, and (c) CHA-4 for 126 days.

of the prism of the CHA-4 group increased at the age of 56 days, which further explained the reason for the decrease in the mechanical properties.

When the age was up to 126 days, the glassy aggregate became a darker-colored reactive ring, the gel-filled cracks widened and stretched into the cement slurry, the aggregate was mostly consumed, and the gel absorbed water and expanded pressure eventually led to aggregate cracking. At this time, the internal damage of the concrete caused by ASR was considered to be serious, and the degradation of the mechanical properties was severe, resulting in the specimen no longer being able to bear the load. The results revealed that the gel filled microcracks and pores, while the number of cracks increased with age and the microcracks extended from the initial defects in the reactive aggregates to the cement matrix. Therefore, the ASR damage could more readily originate from places with initial flaw. And stress concentration as a result of structural defects and the separation of aggregate and cement matrix caused by microcracks may be the major reasons for the progression of ASR failure in reactive aggregates predominantly from the region of initial defects.

5.3.2 Distribution of pore volume

Most classical methods for calculating porosity (including mercury intrusion porosimetry) only obtain information about the total pore content and threshold pore size, but do not obtain the real size and spatial distribution of the pores. However, CT can accurately and non-destructively obtain the volume, distribution of pores, and quantitative data of the samples [31].

The porosity progression of the specimens of the CHA-4 group cured for 7, 56, and 126 days is drawn in Figures 20 and 21, respectively. It can be seen from Figure 21 that the quantity of pores in the specimen progressively reduced with the increase in curing age. As the hydration reaction of cement took place, the hydro-chemical products of cement filled the pores and made the cement matrix more compact. At this point, the ASR gel filled the pores and microcracks of the samples, leading to the reduction of the pore size and porosity of the specimen.

Figure 22(a) and (b) shows the porosity histograms and pore space division of the specimens of the CHA-4 group at 7, 56, and 126 days, respectively. From Figure 22(a), it can be

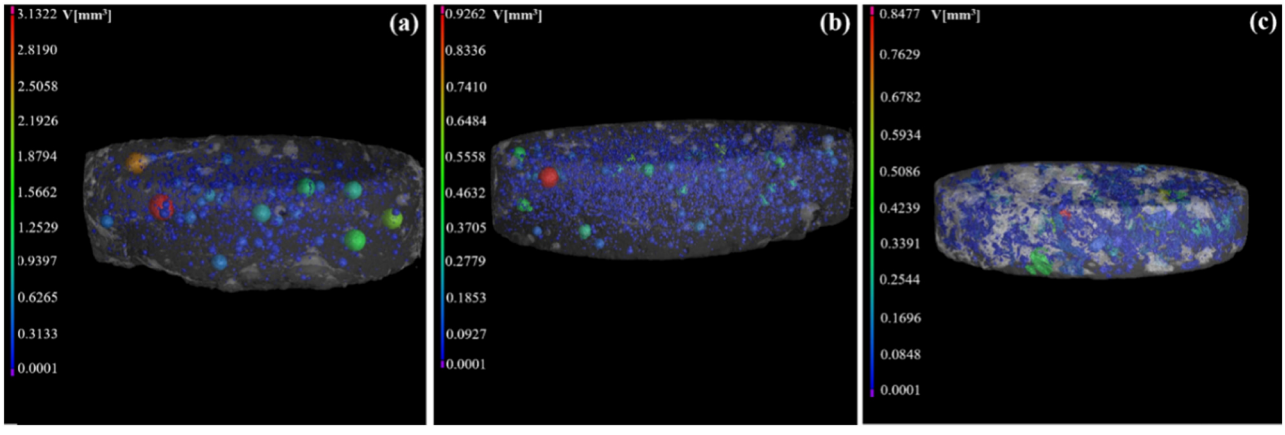

Figure 21: Porosity quantity of the specimen of the CHA-4 group: (a) CHA-4 for 7 days, (b) CHA-4 for 56 days, and (c) CHA-4 for 126 days.

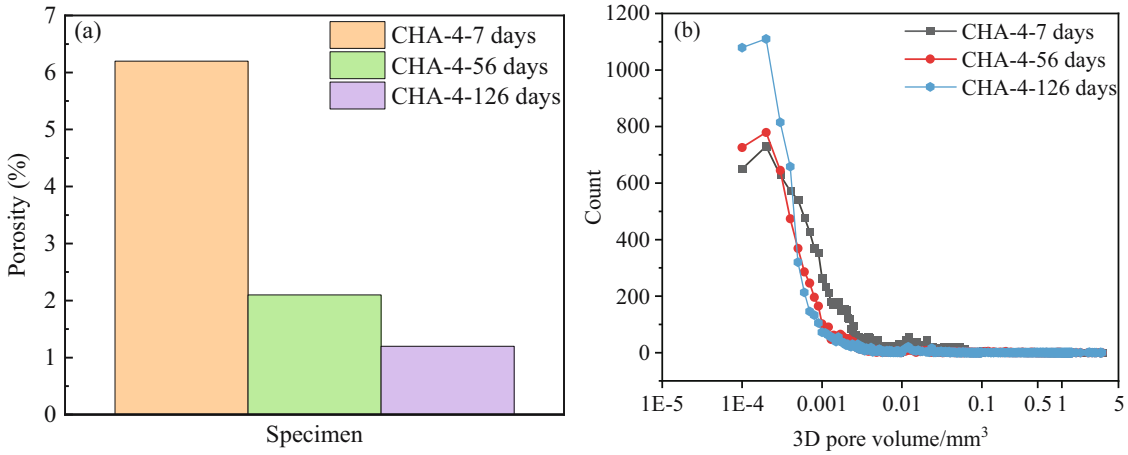

Figure 22: Column diagram about porosity content and pore volume distribution of the CHA-4 group: (a) column diagram about porosity content and (b) pore volume distribution.

quantified that the CHA-4 group specimens had porosities of 6.2, 2.1, and 1.2%, respectively, after maintaining for 7, 56, and 126 days. It could be concluded that the number of big pores and porosity was shown to decrease as the specimen's curing age increased. A significant amount of ASR gel was produced in the prism due to the presence of numerous reactive aggregates therein. And the generated gel continuously filled in the capillary pores; thus, large volume pores gradually became little volume pores, thus leading to smaller porosity of the specimen as the age increased. Besides, it can be observed from Figure 22(b) that the three curves exhibited the same tendency of variation. With the development of curing age, the overall volume of pores declined remarkably, and the pore volume of 0.01–0.1 mm^3 made up the larger percentage.

However, despite the severity of the internal damage to the concrete, the porosity of the specimens did not increase. Consequently, the changes in the samples' porosity do not adequately characterize the situation of internal damage and a reduction in load-bearing capability caused by the ASR of the concrete at an early age.

6 Conclusions

In this study, the concrete prism test, axial compressive test, splitting tensile test, and RDEM test were carried out to investigate the failure criteria of the concrete under the influence of ASR. Additionally, the microscopic morphology and porosity variation of the specimens were evaluated by SEM, X-ray CT scan, and other microscopic means. The following conclusions were drawn:

- The ASR deterioration effect of prism specimens in this study was obvious. And the prisms with high and low dosages of the reactive aggregates would exhibit sharp expansion in the early stage in this study, while the later stage would gradually level off until the reactive aggregates were completely dissolved at the end of the observation period. The increase in the mass of the specimen could not effectively characterize the internal damage caused by ASR, and when the weight gain rate dropped sharply, the degradation of the mechanical properties of the concrete caused by ASR damage was very serious.
- Due to the dominance of cement hydration reaction in the early stages of the test, the effect of continuous cement hydration on strength gain was greater than the influence of ASR-induced damage on the mechanical properties of the concrete. In addition, it was observed that neither of the 28-day ACS and STS of the concrete containing reactive aggregate could effectively reflect the degradation of the mechanical properties caused by ASR. Besides, the weakening effects of the damages caused by ASR on the ACS and RDEM would be stronger, the higher the dosage of reactive aggregates, and at the same time, the STS would be attenuated in advance.
- The most sensitive index for assessing the degree of ASR damage is the RDEM. And RDEM accurately characterizes interior concrete damage to a greater extent as the higher the dosage of reactive aggregates. Based on the RDEM, the ASR failure criteria for concrete at 40°C were determined by comparing and analyzing the indexes such as the ER, the relative ACS, and the relative STS. When the RDEM of concrete with a 3% dosage of reactive aggregates decreases to the range of 70–75%, it is judged that the concrete is destroyed by ASR at this time; when the

RDEM of concrete with a 6% dosage of reactive aggregates decreases to the range of 85–90%, it is judged that the concrete is destroyed by ASR at this time. In practical engineering processes, it is recommended to determine the failure limit of the ER according to the RDEM under the internal damage state.

- The results of SEM revealed that ASR caused many microcracks to form on the reactive aggregates' surface, and the microcracks gradually widened and multiplied over time, causing major internal damage to the concrete and a significant decline in its load-bearing capability. Besides, in accordance with the examination of the X-ray CT scan, the microcracks are more inclined to spread from the initial defects of the aggregate to the cement matrix. And numerous ASR gels formed around the reactive aggregate due to the acceleration of ASR, which continually filled the capillary pores. As time went on, the porosity of the samples decreased. Therefore, the porosity results of CT further confirmed that the bonding force between the ASR gel and the cement matrix after filling pores could not compensate for the loss of the mechanical properties of concrete.

Acknowledgments: This work was supported by the Inner Mongolia Natural Science Foundation of China (Project No. 2019MS05052), the National Natural Science Foundation of China (Project No. 52168032, 52239009, and 51979093) and the Central Support for the Reform and Development of local universities – Discipline Construction – Civil Engineering Quality Cultivation Discipline Construction (Project No. 0404052301).

Funding information: This work was supported by the Inner Mongolia Natural Science Foundation of China (Project No. 2019MS05052) and the National Natural Science Foundation of China (Project No. 52168032, 52239009, and 51979093).

Author contributions: Yongbo Wang: conceptualization, project management, methodology, writing original draft. Peng Gao: data curation, writing review and editing, funding acquisition. Huaizhi Su: methodology, writing review and editing, supervision, funding acquisition. Yuanyu Qin: supervision. Yimeng Wang: conceptualization, supervision. Gang Xue: methodology, funding acquisition, surveillance. All authors have accepted responsibility for the entire content of this manuscript and approved its submission.

Conflict of interest: The authors state no conflict of interest.

References

[1] Figueira, R. B., R. B. Sousa, L. Coelho, M. Azenha, J. M. de Almeida, P. A. Jorge, et al. Alkali-silica reaction in concrete: mechanisms, mitigation, and test methods. *Construction & Building Materials*, Vol. 222, 2019, pp. 903–931.

[2] Diab, S. H., A. M. Soliman, and M. R. Nokken. Changes in mechanical properties and durability indices of concrete undergoing ASR expansion. *Construction & Building Materials*, Vol. 251, 2020, id. 118951.

[3] Islam, M. S. *Performance of Nevada's aggregates in alkali-aggregate reactivity of Portland cement concrete*. Ph.D. thesis, University of Nevada, Las Vegas, NV, 2010.

[4] Rajabipour, F., E. Giannini, C. Dunant, J. H. Ideker, and M. D. A. Thomas. Alkali–silica reaction: Current understanding of the reaction mechanisms and the knowledge gaps. *Cement and Concrete Research*, Vol. 76, 2015, pp. 130–146.

[5] Mohammadi, A., E. Ghiasvand, and M. Nili. Relation between mechanical properties of concrete and alkali-silica reaction (ASR); a review. *Construction & Building Materials*, Vol. 258, 2020, id. 119567.

[6] Vayghan, A. G. and F. Rajabipour. The influence of alkali-silica reaction (ASR) gel composition on its hydrophilic properties and free swelling in contact with water vapor. *Cement and Concrete Research*, Vol. 94, 2017, pp. 49–58.

[7] Vayghan, A. G., F. Rajabipour, and J. L. Rosenberger. Composition–rheology relationships in alkali-silica reaction gels and the impact on the gel's deleterious behavior. *Cement and Concrete Research*, Vol. 83, 2016, pp. 45–56.

[8] Giorla, A. B., K. L. Scrivener, and C. F. Dunant. Influence of viscoelasticity on the stress development induced by alkali-silica reaction. *Cement and Concrete Research*, Vol. 70, 2015, pp. 1–8.

[9] Kawamura, M. and K. Iwahori. ASR gel composition and expansive pressure in mortars under restraint. *Cement Concrete Composites*, Vol. 26, No. 1, 2004, pp. 47–56.

[10] Zhuang, Y., C. Qian, and W. Xu. Calculation of alkali silica reaction (ASR) induced expansion before cracking of concrete. *Journal of the Wuhan University of Technology Materials Science Edition*, Vol. 28, No. 1, 2013, pp. 110–116.

[11] Esposito, R., C. Anac, and M. A. N. Hendriks. Influence of the alkali-silica reaction on the mechanical degradation of concrete. *Journal of Materials in Civil Engineering*, Vol. 28, No. 6, 2016, id. 04016007.

[12] Yurtdas, I., D. Chen, D. W. Hu, and J. F. Shao. Influence of alkali-silica reaction (ASR) on mechanical properties of mortar. *Construction & Building Materials*, Vol. 47, 2013, pp. 165–174.

[13] Pan, J. W., X. Y. Cai, and C. H. Zhang. Mechanism of concrete deterioration caused by alkali-aggregate reaction. *Journal of Water Conservancy*, Vol. 45, No. S1, 2014, pp. 38–42 (In Chinese).

[14] Lu, C. H., S. Z. Bu, Y. L. Zheng, and K. J. Kosa. Deterioration of concrete mechanical properties and fracture of steel bars caused by alkali-silica reaction: A review. *Structures (Oxford)*, Vol. 35, 2022, pp. 893–902.

[15] Ahmed, T., E. Burley, S. Rigden, and A. I. Abu-Tair. The effect of alkali reactivity on the mechanical properties of concrete. *Construction & Building Materials*, Vol. 17, 2003, pp. 123–144.

[16] Abd-Elssamd, A., Z. J. Ma, Y. L. Pape, and N. W. Hayes. Effect of alkali-Silica reaction expansion rate and confinement on concrete degradation. *ACI Materials Journal*, Vol. 117, No. 1, 2020, pp. 265–277.

[17] Saint-Pierre, F., P. Rivard, and G. Ballivy. Measurement of alkali-silica reaction progression by ultrasonic waves attenuation. *Cement and Concrete Research*, Vol. 37, No. 6, 2007, pp. 948–956.

[18] Na, O., Y. Xi, E. Ou, and V. E. Saouma. The effects of alkali-silica reaction on the mechanical properties of concretes with three different types of reactive aggregate. *Structural Concrete*, Vol. 17, No. 1, 2016, pp. 74–83.
[19] Comi, C., R. Fedele, and U. Perego. A chemo-thermo-damage model for the analysis of concrete dams affected by alkali-silica reaction. *Mechanics of Materials*, Vol. 41, No. 3, 2009, pp. 210–230.
[20] Ferche, A. C. and F. J. Vecchio. Mechanical Properties of Alkali-Silica Reaction-Affected Concrete. *ACI Materials Journal*, Vol. 119, No. 1, 2022, pp. 251–262.
[21] Liu, C. X., G. X. Chen, X. J. Wang, and X. Z. Kong. The effect of ASR on concrete mechanical properties. *Journal of China Institute of Water Resources and Hydropower Research*, Vol. 10, No. 2, 2012, pp. 105–111 (In Chinese).
[22] Swamy, Y. N. *The Alkali-Silica reaction in concrete*. Van Nostrand Reinhold, New York, Blackie, 1992.
[23] Giaccio, G., R. Zerbino, J. M. Ponce, and O. R. Batic. Mechanical behavior of concretes damaged by alkali-silica reaction. *Cement and Concrete Research*, Vol. 38, No. 7, 2008, pp. 993–1004.
[24] Marzouk, H. and S. Langdon. The effect of alkali-aggregate reactivity on the mechanical properties of high and normal strength concrete. *Cement and Concrete Composites*, Vol. 25, No. 4–5, 2003, pp. 549–556.
[25] Gao, P., Y. B. Wang, and G. Xue. Influence of waste rubber powder, polypropylene fiber and binary blends with them on mitigating alkali-silica reaction. *Journal of Building Engineering*, Vol. 67, 2023, id. 105951.
[26] GB/T 1346-2011. *Test methods for water requirement of normal consistency setting time and soundness of the Portland cement*. National Standards of the People's Republic of China, 2011.
[27] GB/T SL 352-2020. *Test code for hydraulic concrete*. Ministry of Water Resources of the People's Republic of China, 2020.
[28] GB/T 14685-2011. *Standard for test methods of pebble and crushed stone for construction*. National Standards of the People's Republic of China, 2011.
[29] GB/T 50082-2009. *Standard for test methods of long-term performance and durability of ordinary concrete*. National Standards of the People's Republic of China, 2009.
[30] GB/T 50081-2019. *Standard for test methods of concrete physical and mechanical properties*. National Standards of the People's Republic of China, 2019.
[31] Baruchel, J., J. Y. Buffiere, E. Maire, and P. Merle. *X-ray tomography in material science*, Butterworth-Heineman, 2000.
[32] ASTM C1260-14. *Standard Test Method for Potential Alkali Reactivity of Aggregates (Mortar-bar Method)*. West Conshohocken, PA, 2014.
[33] Liu, C. X. *Experimental investigation on suppression and expansion prediction of alkali-silica reaction in concrete*. China Institute of Water Resources and Hydropower Research, 2006 (In Chinese).
[34] Islam, M. S. and N. Ghafoori. Relation of ASR-induced expansion and compressive strength of concrete. *Materials and Structures*, Vol. 48, No. 12, 2015, pp. 4055–4066.
[35] Multon, S. and F. Toutlemonde. Effect of moisture conditions and transfers on alkali silica reaction damaged structures. *Cement and Concrete Research*, Vol. 40, No. 6, 2010, pp. 924–934.
[36] Gong, F., Y. Takahashi, I. Segawa, and K. Maekawa. Mechanical properties of concrete with smeared cracking by alkali-silica reaction and freeze-thaw cycles. *Cement and Concrete Composites*, Vol. 111, 2020, id. 103623.
[37] Sanchez, L. F. M., B. Fournier, M. Jolin, D. Mitchell, and J. Bastien. Overall assessment of Alkali-Aggregate Reaction (AAR) in concretes presenting different strengths and incorporating a wide range of reactive aggregate types and natures. *Cement and Concrete Research*, Vol. 93, 2017, pp. 17–31.
[38] Gautam, B. P., D. K. Panesar, S. A. Sheikh, and F. J. Vecchio. Effect of coarse aggregate grading on the ASR expansion and damage of concrete. *Cement and Concrete Research*, Vol. 95, 2017, pp. 75–83.
[39] Xu, X. C. *Study on the mechanism of concrete alkali silica reaction under multiple factors*. Zhejiang University of Technology, 2014 (In Chinese).
[40] Sha, J. F., W. Sun, B. G. Zhan, and T. Y. Li. Damage characteristics of concrete under two-fold factors of ASR and chloride corrosion. *China Concrete and Cement Products*, Vol. 01, 2006, pp. 4–7.
[41] GB/T 50476-2019. *Standard for the design of concrete structure durability*. National Standards of the People's Republic of China, 2019.
[42] Hong, S. Y. and F. P. Glasser. Alkali binding in cement pastes Part I. The C-S-H phase. *Cement and Concrete Research*, Vol. 29, No. 12, 1999, pp. 1893–1903.
[43] Dupuis, R. and R. J. M. Pellenq. Alkali silica reaction: A view from the nanoscale. *Cement and Concrete Research*, Vol. 152, 2022, id. 106652.
[44] Shi, Z. G. and B. Lothenbach. The role of calcium on the formation of alkali-silica reaction products. *Cement and Concrete Research*, Vol. 126, 2019, id. 105898.
[45] Fanijo E. O., E. Kassem, and A. Ibrahim. ASR mitigation using binary and ternary blends with waste glass powder. *Construction and Building Materials*. Vol. 280, 2021, id. 122425.